

Quadratic Mixing of Radio Frequency Signals using Superconducting Quantum Interference Filters

P. Caputo, J. Tomes, J. Oppenländer, Ch. Häussler, A. Friesch, T. Träuble, and N. Schopohl^a

Lehrstuhl für Theoretische Festkörperphysik, Universität Tübingen

Auf der Morgenstelle 14, 72076 Tübingen (Germany)

(Dated: April 14, 2024)

The authors demonstrate quadratic mixing of weak time harmonic electromagnetic fields applied to Superconducting Quantum Interference Filters, manufactured from high- T_c grain boundary Josephson junctions and operated in active microcooler. The authors use the parabolic shape of the dip in the dc-voltage output around $B = 0$ to mix *quadratically* two external rf-signals, at frequencies f_1 and f_2 well below the Josephson frequency f_J , and detect the corresponding mixing signal at $|f_1 - f_2|$. Quadratic mixing takes also place when the SQIF is operated without magnetic shield. The experimental results are well described by a simple analytical model based on the adiabatic approximation.

Superconducting Quantum Interference Filters (SQIFs) are Josephson junction (JJ) interferometers that sense, when operated in the resistive mode, the presence of a magnetic field B by transforming it to a characteristic dc voltage output $V_{dc}(B)$. Upon sweeping a control current through a coil to generate a suitable compensation field, the voltage output of a SQIF shows a pronounced unique dip around zero total static field $B = 0$. The dip of a SQIF is characterized by its width ΔB and its voltage swing ΔV [1, 2]. The detailed shape of the voltage output $V_{dc}(B)$ can be engineered by choosing suitable areas of the SQIF loops. The performance of a SQIF is only weakly sensitive to the spread of the JJ parameters. These features make SQIFs interesting for applications with ceramic cuprate superconductors. The sensitivity of a SQIF in response to an applied magnetic field is determined by the *voltage-to-magnetic field* transfer factor $V_B = \max(\partial V_{dc}/\partial B)$. For example, in a serial SQIF array with N loops the transfer factor V_B scales with N , but the voltage noise $\overline{S_V}$ derived from the spectral density S_V (white noise) scales with \sqrt{N} , so that the dynamic range $V = \overline{S_V}$ varies proportional to \sqrt{N} [3, 4]. Employing various flux focusing structures together with a SQIF it is possible to significantly enhance the transfer factor [5, 6]. A flux focusing structure integrated together with a SQIF (SQIF-sensor) is sketched in Fig. 1(c).

In the resistive state, the working point of the device is set by a bias current I_b and also by a static field B . The dc voltage output $V_{dc}(B)$ of the SQIF is the time average of a fast signal $V(B; t) / \partial \varphi = \partial t$, where φ is the Josephson phase across the JJ. The main harmonic of $V(B; t)$ has frequency $f_J = V_{dc}(B) / \phi_0$ (the second Josephson relation) [7]. In the presence of additional weak radiofrequency magnetic field $b_{rf}(t)$ which varies slowly in comparison with f_J , the SQIF voltage can be written as

$$\begin{aligned} hV(B + b_{rf}(t); t) &= \\ &= V_{dc}(B) + V_{dc}^0(B) \cdot \frac{1}{2} V_{dc}^0(B) \cdot \frac{1}{2} V_{dc}^0(B) \cdot \frac{1}{2} V_{dc}^0(B) + \dots; \end{aligned} \quad (1)$$

where prime denotes the derivative with respect to B , and h

the time average over the time scale set by f_J^{-1} , while the slow time dependence remains. For $b_{rf}(t) = b_1 \cos(2\pi f_1 t)$, with amplitude $b_1 \ll B$ and frequency $f_1 < \frac{f_J}{2}$, Eq. (1) describes a superposition of the dc voltage output $V_{dc}(B)$ with a slowly varying *rf* voltage output at frequencies $f_1, 2f_1$, etc. The amplitude of the first harmonic of the Fourier spectrum of the output signal contains information about the slope $V_{dc}^0(B)$, while the amplitude of the second harmonic is proportional to the curvature $V_{dc}^0(B)$.

The Fourier transform of $V(B + b_{rf}(t); t)$ is the *spectral voltage output* $\tilde{V}(B; f)$. The power spectrum $\tilde{V}(B; f)^2$ vs. B can be detected at frequencies around the center frequency f_1 using a spectrum analyzer. If $b_1 \ll B$, the spectral voltage output will be proportional to $V_{dc}^0(B)$: it will be maximum in field regions of maximum slope, while in regions of a flat $V_{dc}(B)$ curve, say around $B = 0$, it will tend to zero.

Quadratic mixing is expected for two tone experiments, where the incident *rf* signal is a superposition of two time harmonic signals: $b_{rf}(t) = b_1 \cos(2\pi f_1 t) + b_2 \cos(2\pi f_2 t)$ (we assume $f_1, f_2 < \frac{f_J}{2}$). Taking into account the parabolic shape of the $V_{dc}(B)$ -curve around $B = 0$, one expects in that region a larger amplitude for the quadratic mixing signals at frequencies $f_2 - f_1, 2f_1, f_2 + f_1$ and $2f_2$, respectively, compared to the field regions where $V_{dc}^0(B)$ is maximal (zero curvature).

Previously we reported on *dc* experiments with SQIF-sensors in shielded and also in unshielded active micro-coolers [4, 8, 9]. Active cooling offers numerous advantages: possibility to choose stable temperature down to 50 K, quick thermal cycles, and compact and portable setups [10]. Results obtained in unshielded micro-coolers have never revealed a significant degradation of the SQIF-sensor performance with respect to shielded micro-coolers. We believe the principal reason for this is the large dynamic range of the SQIF's.

In the current experiments we broadcast an *rf*-signal, representing a superposition of two time harmonic fields, with $f_1, f_2 < \frac{f_J}{2}$ and small amplitudes b_1 and b_2 , to a SQIF-sensor mounted inside the micro-cooler. The measured spectral voltage output $\tilde{V}(B; f)$ of the SQIF is shown in Figs. 2–3. One clearly recognizes besides the primary signals at frequencies f_1 and f_2 , a quadratic mixing signal at frequency $f_1 - f_2$, with a maximum amplitude when the SQIF is tuned at the bottom of the dip at $B = 0$. For increasing field B , the amplitude

^aElectronic address: nils.schopohl@uni-tuebingen.de

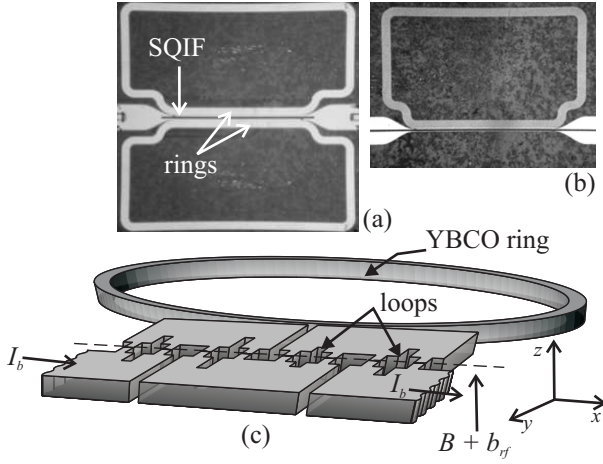


FIG. 1: (a) Optic microscope image of the chip with the SQIF at the center of the substrate, and the two rings, inductively coupled to the SQIF; (b) SQIF sensor with one ring. All superconducting parts, except the regions across the junctions, are covered by gold. (c) Sketch, not in scale, of the SQIF-sensor. The dashed line indicates the grain boundary.

of the quadratic mixing signal symmetrically decreases and apparently vanishes under the noise floor of the detector as a function of B at approximately half-way to the position of maximal dip slopes. In sharp contrast to this behavior, both first order signals display a maximum amplitude there where the dip slope is maximal. The effect is observed for various SQIF-sensors, with different critical current densities, always with a strenght that increases with the increase of the transfer factor V_B . In all cases, Eq.(1) provides an excellent description of the detected spectral voltage output vs. static field B .

The Josephson junctions in our arrays consist of $\text{YBa}_2\text{Cu}_3\text{O}_{7-x}$ grain boundary junctions grown on 24-oriented bicrystal MgO substrates[11]. They are designed with a width of $2 \text{ } \mu\text{m}$, the $\text{YBa}_2\text{Cu}_3\text{O}_{7-x}$ layer being 130 nm thick, so that the resulting junction critical current density is $J_c = 23 \text{ kA}/\text{cm}^2$, at $T = 77 \text{ K}$. The serial SQIF consists of 211 loops, the distribution of the loop areas ranging between $38 \text{ } \mu\text{m}^2$ and $210 \text{ } \mu\text{m}^2$. In order to vary the coupling of magnetic flux into the SQIF, we designed two types of focusing structures. Type (a) consists of two superconducting rings being symmetrically placed on both sides of the grain boundary [Fig. 1(a)]. Type (b) is made with only one superconducting ring [Fig. 1(b)]. Type (b) is effectively a split loop design[12], consisting of 10 equidistant parallel thin loops, one aligned inside the other. The static magnetic field B is applied via a multi-turn coil placed inside the cooler. The rf field $b_{rf}(t)$ is applied via a 50-loop antenna. Experiments are made either with a mu-metal shield - in this case the rf antenna was placed inside the shield at a distance of about 5 cm from the chip -, or with an unshielded cryocooler in open space.

We first discuss the experiments with shielded cryo-cooler. We measure the $V_{dc}(B)$ dependence of the SQIF, and check the dip symmetry with respect to zero field. There is an optimal temperature at which the voltage swing is a maximum, at a properly chosen I_b . At $T = 76 \text{ K}$, the SQIF critical

current is $I_c = 50 \text{ A}$ and, at $I_b = 85 \text{ A}$, we measure $V = 1160 \text{ V}$ and $V_B = 6500 \text{ V} = T$. The SQIF normal resistance is $R = 186 \text{ } \Omega$. Successively, the rf is switched on: a time harmonic signal is applied to the primary antenna, while the SQIF rf output is detected. The value b_1 is chosen much smaller than B , to ensure that the rf signal superimposed to the static field does not modulate the SQIF working point out of the dip and corrupt the effect; but it has to be high enough so that the spectral voltage output is above the noise level set by the resolution bandwidth (ResBW) of the spectrum analyzer.

In the single tone rf experiment, the incident signal has frequency $f_1 = 102 \text{ MHz}$ and amplitude $b_1 = 23 \text{ dBm}$. At $I_b = 58 \text{ A}$ and $T = 75 \text{ K}$, the voltage swing is about $400 \text{ } \mu\text{V}$. The SQIF rf voltage is amplified by a cold amplifier, designed with high input resistance ($5 \text{ k}\Omega$). The spectrum analyzer is operated as a narrowband receiver tuned at frequency $f' = f_1$, with a bandwidth set by the ResBW (*zero span mode*), so that the analog output corresponds to the maximum signal amplitude. The ResBW is varied from 3 kHz to 1 MHz . The spectral voltage output of the SQIF is recorded by computer while slowly sweeping the static field B (sweep frequency in the kHz range). Simultaneously the $V_{dc}(B)$ curve is acquired. Figure 2(a) displays typical results. Here the 0 dB level is arbitrary, being at the present the amplifier gain not exactly known. It is found that, at frequency f_1 , the spectral voltage output of the SQIF vs. B is a maximum in field regions where the dip slopes are maximal. In Fig.2(b) we plot the modulus of the first derivative of the theoretically calculated voltage output vs. magnetic field B and bias current I_b .

In the two tone rf experiments, the incident field is a linear combination of two signals with frequency $f_1 = 220 \text{ MHz}$ and $f_2 = 100 \text{ MHz}$, and amplitude $b_1 = b_2 = 22 \text{ dBm}$. In the spectral voltage output of the SQIF, we find then a quadratic mixing signal at the difference frequency $f = f_1 - f_2 = 120 \text{ MHz}$. The amplitude of this signal is maximal at $B = 0$. Figure 3(a) displays the spectral voltage output detected at $f = 120 \text{ MHz}$, with ResBW equal to 3 kHz . Symmetrically, at $f = f_1 + f_2 = 320 \text{ MHz}$ a similar spectral voltage response is detected. In the current set-up, quadratic mixing has been observed up to few GHz. In Fig.3(b) we plot the theoretically calculated $\partial V_{dc}^0(B)/\partial B$ vs. B and vs. I_b .

In the rf experiments without magnetic shield, the environmental disturbances do not suppress the dip (although in this case the compensation field is different), and the quadratic mixing effect as well as the second harmonic generation take place, similar to the results obtained with the shielded cooler. In the single tone experiment with a time harmonic rf signal at frequency f_1 , we also detected second harmonic signal generation at $2f_1$ in the spectral voltage output of the SQIF-sensor, with a field dependence around $B = 0$ as shown in Fig.3(a).

In conclusion, we have demonstrated that a SQIF-sensor is capable to transfer the modulations of an incident time harmonic electromagnetic signal with carrier frequency $f_1 < \frac{f_J}{2}$ into a corresponding rf voltage output. This suggests potential applications of a SQIF as a non-linear mixing device, capable to operate at frequencies from dc to few GHz with a large dynamic range. All experiments have shown that the strength of the rf voltage output at frequency f_1 depends crucially on the

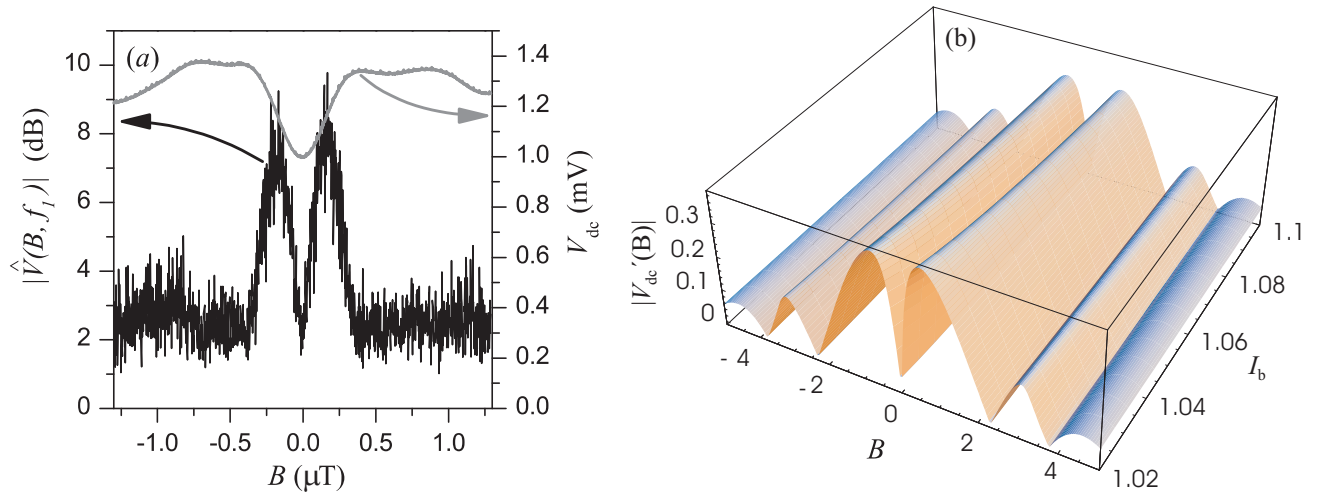


FIG. 2: (a) SQIF dc voltage V_{dc} at $I_b = 58$ A and $T = 75$ K vs. static magnetic field B (gray curve, relative to right axis); simultaneous measurements of the maximum amplitude of the SQIF rf voltage $\hat{\psi}(B; f_1)$, induced by the rf field with $f_1 = 102$ MHz and $b_1 = 23$ dBm (black curve, relative to left axis). Detection is made by spectrum analyzer in zero span mode, at f_1 and with ResBW = 3 kHz. The 0 dB level is arbitrary. (b) Modulus of the first derivative of V_{dc} vs. static field and bias current.

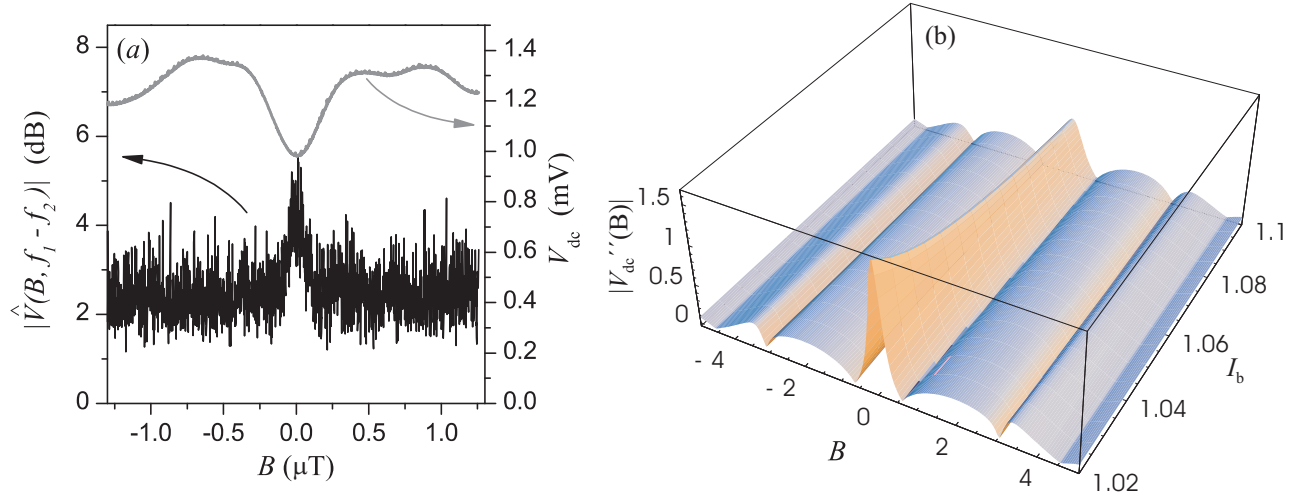


FIG. 3: (a) Gray curve, relative to right axis: V_{dc} vs. B ; black curve, rel. to left axis: rf voltage $\hat{\psi}(B; f_1)$ detected at $f_1 - f_2 = 120$ MHz, with a ResBW of 3 kHz. The 0 dB level is arbitrary. The main signals were at $f_1 = 220$ MHz and $f_2 = 100$ MHz; amplitudes $b_1 = b_2 = 22$ dBm. (b) Modulus of the second derivative of V_{dc} vs. static field and bias current.

slope of the $V_{dc}(B)$ curve: SQIF-sensors with smaller transfer factor V_B have a reduced maximum amplitude in their rf voltage output.

The authors are most grateful to R. IJsselsteijn to provide

us with samples of various critical current densities, and thank V. Schultze for sharing his insight and many useful discussions.

-
- [1] J. Oppenländer, Ch. Häussler, and N. Schopohl, Phys. Rev. B, **63**, 024511 (2000).
 - [2] Ch. Häussler, J. Oppenländer, and N. Schopohl, J. Appl. Phys., **89**, 1875 (2001).
 - [3] J. Oppenländer, P. Caputo, Ch. Häussler, T. Träuble, J. Tomes, A. Friesch, and N. Schopohl, Appl. Phys. Lett., **83**, 969 (2003).
 - [4] J. Oppenländer, Ch. Häussler, A. Friesch, J. Tomes, P. Caputo, T. Träuble, and N. Schopohl, IEEE Trans. Appl. Supercond., **15**, 936 (2005).
 - [5] V. Schultze, R. IJsselsteijn, R. Boucher, H.-G. Meyer, J. Oppenländer and Ch. Häussler, and N. Schopohl, Supercond. Sci. Technol., **16**, 1356 (2003).

- [6] V. Schultze, R. IJsselsteijn and H.-G. Meyer, *Supercond. Sci. Technol.*, **19**, 411 (2006).
- [7] A. Barone and G. Paternò, *Physics and Applications of the Josephson Effect*, J. WILEY & SONS, New York (1982).
- [8] P. Caputo, J. Oppenländer, Ch. Häussler, J. Tömes, A. Friesch, T. Träuble, and N. Schöpohl, *Appl. Phys. Lett.*, **85**, 1389 (2004).
- [9] P. Caputo, J. Tömes, J. Oppenländer, Ch. Häussler, A. Friesch, T. Träuble, and N. Schöpohl, *IEEE Trans. Appl. Supercond.*, **15**, 1044 (2005).
- [10] AIM, AEG Infrarot-Module GmbH, Heilbronn, Germany.
- [11] Institute for Physical High Technology (IPHT), Jena, Germany.
- [12] F. Ludwig, A. B. M. Jansman, D. Drung, M. O. Lindström, S. Bechstein, J. Beyer, J. Flokstra, and T. Schurig, *IEEE Trans. Appl. Supercond.*, **11**, 1315 (2001).